Structural and Vibrational Study of $[Mo_7O_{24}]^{6-}$ and $[W_7O_{24}]^{6-}$

Blandine Courcot* and Adam J. Bridgeman

School of Chemistry, University of Sydney, 2006 NSW, Australia

Received: July 5, 2009; Revised Manuscript Received: July 29, 2009

Density functional methods have been used to investigate the structure and the vibrational modes of $[M_7O_{24}]^{6-}$ isopolyanions of molybdenum and tungsten. Relativistic effects have been considered through the zeroth-order regular approximation (ZORA) and interactions with an aqueous environment modeled by the COSMO approach. A structural study of the two compounds has been performed, and the geometrical parameters obtained are in good agreement with experimental data. However, when the solvent is introduced in the model, deviations are found, especially for some tungsten−oxygen bonds which involve pseudoterminal oxygens. Thus, different computational strategies have been tested to reject any reliance on the COSMO model and the optimization algorithms. The variations compared to solid-state bond lengths appear to be due to the solvent. Infrared and Raman spectra have been also calculated in the gas phase and in water leading, for the first time, to a detailed assignment of the vibrational frequencies. The vibrational contributions of the aminopyridinium counterion $[C_5H_7N_2]^+$ have been isolated, improving the assignment of experimental spectra. Inclusion of solvent causes a shift toward lower frequencies and an increase in the intensity of the peaks. Spectra obtained using pseudo-gas-phase calculations reproduce the experimental data most satisfactorily, especially when the experiments are performed on the solid state.

Introduction

Primarily built by edge- and, sometimes, corner-sharing of MO_6 octahedra, polyoxometalates form a class of inorganic compounds with applications in various fields from material science to medicine.[1,2] Most of their uses are based on properties which depend on their size, mass, and charge, their ability to transfer electrons and protons, the lability of "lattice oxygen", and their high Bronsted acidity.[2] Infrared and Raman spectroscopy are undoubtedly good tools in understanding these properties, both in the solid state and solution. Compared to the large number of metal−oxygen cluster anions, relatively few detailed spectroscopy experiments have been performed. This motivates the need for reliable calculated spectra starting from an optimized geometry of the anions. Clusters of molybdenum(VI) and tungsten(VI) such as heptamolybdate $[Mo_7O_{24}]^{6-}$ and heptatungstate $[W_7O_{24}]^{6-}$ represent simple models for larger polymeric systems.[1,2]

Previous studies on octamolybdate isomers have shown that the coordination number of oxygen atoms is very sensitive to the environment, with three-coordinated atoms in isolated anions tending to become four-coordinated when they interact with their environment such as with a counterion.[3] The hepta-anion possesses pseudo-terminal oxygen atoms which could have a similar behavior. They are formally bonded to two metal atoms, creating one long and one short bond. Because this short bond is closer to the bond length of the metal−terminal oxygen bond, they have been called pseudoterminal atoms.[4] Their influence on polyanions' reactivity and spectroscopic properties is not well understood.

In this paper, the necessity for inclusion of solvent effects when studying the structural and vibrational properties of polyanions is investigated. The pseudoterminal atoms distinctive to the hepta-anions appear to interact differently with the solvent, especially when comparing with the bridging and terminal oxygens. The sensitivity of type-II POMs to the environment will be analyzed. This analysis will then also consider the aminopyridinium counterion $[C_5H_7N_2]^+$ as part of the solid-state environment. The calculated vibrational modes will include the contribution of both the anion and the cation, leading to an assignment of the frequencies directly comparable with experiments made on crystals. This attempt to mimic the environment of heptatungstate and heptamolybdate, in solution or in crystals, relies on an adapted and pragmatic computational strategy that will be discussed as well when reporting the results.

Computational Method

Previous structural studies on hexa- and heptapolyanions have shown that density functional methods lead to results in good agreement with experimental data.[5,6] Several DFT approaches have been also tested on isopolyanions and heteropolyanions to determine their ability to reproduce vibrational frequencies.[7−10] These studies marked the very first attempts to assign the vibrational spectra of polyoxometalates based on high-level calculations and covered type-I and type-II polyanions as well as iso- and heteropoly systems. The heptamolybdate and heptatungstate systems are type-II systems as they possess *cis*-MO_2 oxo units. However, they also possess pseudoterminal oxo groups and have distinctly lower symmetry than the ions previously studied. As is common for polyoxometalates, these ions have been commonly stabilized by crystallization with large organic cations. This paper is thus motivated by the need to assign the characteristic vibrations for this class of polyanion and to assess the suitability of the computational methodology in treating low-symmetry polyanions in the presence of other species.

For consistency with these previous studies, functionals based on the Vosko−Wilk−Nusair (VWN) form of the local density approximation were employed.[11] Slater-type orbital (STO) basis sets of triple-ζ quality with frozen cores were chosen (in ADF:

* To whom correspondence should be addressed. E-mail: b.courcot@chem.usyd.edu.au.

10.1021/jp9063438 CCC: $40.75
Published on Web 09/08/2009

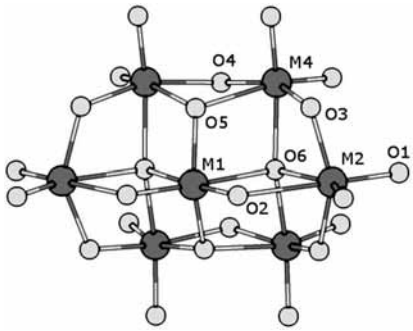

Figure 1. Structure and atom labeling for the polyanion $[M_7O_{24}]^{6-}$.

O 1s, Mo 3d, and W 4f). Some calculations, reported as Supporting Information, were also performed with the generalized gradient approximation using Becke's 1988 exchange[12] and Perdew's 1986 correlation[13] corrections (BP86). All calculations were performed with the ADF program, version 2008.[14−16] It is worth noting that the geometry optimization algorithm was improved[17] in this version of the code and is now used as default.

Relativistic effects were incorporated through the zeroth-order regular approximation.[18−20] Each calculation was performed including either only scalar effects or spin−orbit coupling as well.

Interactions with solvent were processed using the COSMO approach available in ADF.[21,22] To construct the solvent-excluding surface, the default Allinger van der Waals radii were preferred ($r_O = 1.52$ Å and $r_M = 1.99$ Å), but some calculations were also run with a smaller radius for the metal atoms ($r_{Mo} = 0.74$ Å, $r_W = 0.99$ Å). The Klamt surface was also tested for the solvent-accessible surface.[21] For most calculations, the dielectric constant was set to 78, which corresponds to an aqueous environment at a temperature of 20 °C. Calculations were also performed using a range of dielectric constants to investigate the influence of the environment on the pseudoterminal oxygen atoms.

The Infrared and Raman spectra were calculated with the scalar ZORA, and both numerical and analytical frequencies were obtained. Spin−orbit coupling was considered only through a numerical approach. The two types of frequencies were compared when it was possible, except for the COSMO calculations, where only the numerical frequencies were available. Gradient convergence criteria and integration accuracies were both set to 10^{-5}.

Results and Discussion

Structure of the $[Mo_7O_{24}]^{6-}$ and $[W_7O_{24}]^{6-}$ Anions. ***Geometry in the Gas Phase.*** A structural scheme showing atom labels is presented in Figure 1. Hepta-anions show three different types of metal centers, labeled here as M_1, M_2, and M_4, and four groups of oxygen sites, terminal oxygen (O_t: O_1), two-coordinate (O_{2c}: O_2, O_3, O_4), three-coordinate (O_{3c}: O_5), and four-coordinate (O_{4c}: O_6) atoms. Calculated M−O bond distances for the two anions $[Mo_7O_{24}]^{6-}$ and $[W_7O_{24}]^{6-}$ in the gas phase and including the solvent are given in Table 1. Experimental bond lengths, taken from Tytko et al. for the heptamolybdate[4] and from Ikenoue et al. for the heptatungstate,[23] are included in parentheses. They were also used as references in a study by Bridgeman and Cavigliasso, where all of the calculations were performed choosing only the scalar ZORA approach.[5] Both polyanions are predicted to have C_{2v} symmetry, as observed in the crystalline phase. It should be first noted that atom O_2 is a two-coordinate site but the M_1-O_2 bond length is predicted to be 1.77 Å, which is closer to a $M-O_t$ distance than to a $M-O_{2c}$ distance. As defined in the Introduction, this oxygen atom is described as a pseudoterminal atom O_{pt}.

TABLE 1: Optimized M−O Distances in the Gas Phase and Including the Aqueous Solvent (in Å)[a]

		$[Mo_7O_{24}]^{6-}$			$[W_7O_{24}]^{6-}$		
parameter		gas phase	solvent		gas phase	solvent	
$M-O_t$	M_1-O_1	1.76	1.74	(1.72)	1.76	1.74	(1.74)
$M-O_{2c}$	M_1-O_2	1.77	1.77	(1.74)	1.77	1.77	(1.77)
	M_2-O_2	2.47	2.44	(2.52)	2.47	2.37	(2.48)
	M_2-O_3	1.91	1.92	(1.92)	1.91	1.91	(1.90)
	M_4-O_3	2.00	1.97	(1.98)	1.99	1.96	(1.98)
	M_4-O_4	1.93	1.93	(1.93)	1.93	1.93	(1.95)
$M-O_{3c}$	M_1-O_5	1.89	1.89	(1.90)	1.88	1.89	(1.89)
	M_4-O_5	2.29	2.24	(2.27)	2.28	2.23	(2.28)
$M-O_{4c}$	M_1-O_6	2.31	2.23	(2.26)	2.29	2.19	(2.26)
	M_2-O_6	2.18	2.15	(2.16)	2.18	2.19	(2.20)
	M_4-O_6	2.16	2.15	(2.16)	2.16	2.15	(2.17)

[a] Experimental results are given in parentheses for comparison.[4,23]

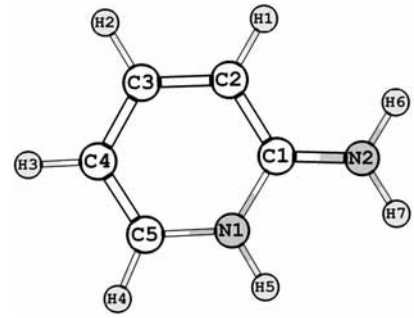

Figure 2. Structure for the aminopyridinium cation.

Carrying out computations on molecules containing heavy nuclei leads to the necessity of considering relativistic effects on calculations. The zeroth-order regular approximation (ZORA) is by far the most frequently used methodology.[18−20] Nevertheless, for the two hepta-anions, the largest difference between the bond lengths obtained using scalar and spin−orbit coupling ZORA bond lengths is 0.01 Å. This small difference is found for Mo_4-O_5, Mo_1-O_6, and Mo_4-O_6 in heptamolybdate but only for W_2-O_2 in heptatungstate. Therefore, even for the heptatungstate, which contains atoms with an atomic number of 74, the influence of the spin−orbit coupling on the geometry is very small. Variations from the experimental data are more linked to the level of theory used for the calculations (as shown in Figure 7, Supporting Information) than the consideration of the spin−orbit coupling. Spin−orbit coupling has only a small influence on the structure of these molecules and could be neglected for geometry optimization.

Figure 2 shows the structure of the aminopyridinium counterion $[C_5H_7N_2]^+$. Table 2 lists the results of a geometry optimization performed at the same level of theory as that used for the polyanions. The results are compared with the solid-state data from Román and co-workers. Good agreement is obtained, even though theoretical calculations correspond to an isolated gas-phase cation. The largest deviation occurs for the bonds N_1-C_1 and C_4-C_5.

Effect of the Solvent. Another important aspect in the computational strategy for POMs is to consider interactions with their environment. López and co-workers have underlined the "strict necessity" to incorporate solvent effects when the ratio $q/m \geq 0.8$, where q is the charge of the polyoxoanion and m is the number of metal centers in the polyanion.[25] With a ratio equal to 0.86, $[M_7O_{24}]^{6-}$ anions are good candidates.

TABLE 2: Optimized Distances (in Å) for the Aminopyridinium $[C_5H_7N_2]^+$ Cation Obtained with a Spin−Orbit Coupling ZORA Calculation in the Gas Phase[a]

parameter	bond length
C_1-C_2	1.40 (1.40)
C_2-C_3	1.37 (1.37)
C_3-C_4	1.40 (1.40)
C_4-C_5	1.36 (1.34)
C_5-N_1	1.35 (1.36)
N_1-C_1	1.35 (1.37)
N_2-C_1	1.33 (1.33)

[a] Experimental distances are given in parentheses.[24]

For $[W_7O_{24}]^{6-}$, López and co-workers reported a general shortening of interatomic distances caused by the solvent. In comparison to hexaniobate $[Nb_6O_{19}]^{8-}$, they added that hexatungstate $[W_6O_{19}]^{2-}$, for example, was "almost unchanged" by the effects of the aqueous solvent, in agreement with the conclusion obtained by Bridgeman for the $[TeMo_6O_{24}]^{6-}$ and $[IMo_6O_{24}]^{6-}$ Anderson polyanions.[10] Bagno and co-workers found bond lengths shorten upon hydration for W−O, reducing by 0.003 Å for $W-O_b$ and by 0.009 Å for $W-O_t$.[26] Table 1 confirms this decrease of M−O bonds distances due to the solvent, with an improvement in $W-O_t$ bonds from 1.76 to 1.74 Å, almost equal to the experimental value. However, three tungsten−oxygen bonds are much more sensitive to the solvent, W_2-O_2, W_4-O_5, and W_1-O_6. These bonds involve two-, three-, and four-coordinate oxygen atoms, respectively. Interestingly, these bonds are also the most sensitive to the level of theory used, in particular, to the GGA approach (the comparison is plotted on Figure 7, Supporting Information).

To investigate further the effect of the solvent model, several geometry optimizations were performed with different dielectric constants to mimic different solvent polarities, $\varepsilon = 2$ for cyclohexane, $\varepsilon = 6.19$ for acetic acid, $\varepsilon = 20$ for acetone, $\varepsilon = 37.5$ for acetonitrile, and $\varepsilon = 182.4$ C^2 J^{-1} m^{-1} for methylformamide. The decrease of W_2-O_2, W_4-O_5, and W_1-O_6 bond lengths with the increase of ε was confirmed. Inclusion of even a nonpolar solvent such as cyclohexane leads to a large change in the bond length. The effect of polar solvents is only slightly worse and becomes constant around the dielectric constant of acetonitrile.

Finally, to check the influence of the accessible COSMO surface on the geometry, the Klamt surface was also tested, and smaller radii for metal atoms were picked. The two surfaces differ by the value of the solvent radius, which is set to 1.93 Å for the solvent-excluding surface and 3.64 Å for the Klamt surface. The choice of a smaller metal radius was motivated by the study of Fernández and co-workers,[27] where they fixed it to 0.74 Å. Results show that only metal−terminal oxygen bonds are affected by the change of metal radii, with a variation of 0.02 Å. Since interaction distances between the solvent and the anion are in that case shorter, it is not surprising that it is the bonds to the terminal oxygen atoms (the most exposed to water molecules) that are the most sensitive. López and co-workers have shown, based on molecular dynamics simulations, that for the α-$[PW_{12}O_{40}]^{3-}$ Keggin anion, the region with greatest accumulation of water molecules is located at 6−9 Å from the center of the cluster, resulting in the highest solvation for terminal oxygen atoms in comparison with bridging atoms.[28] They used the SPC/E model[29] to simulate the solvent. This discrete arrangement of water molecules was investigated recently by P. Jaramillo and co-workers.[30] They emphasized the limits of a continuum approach such as PCM on the prediction of chemical quantities based on the frontier orbitals. A discrete approach might improve the consideration of the solvent, but it will either greatly increase the computational cost if DFT is used or rely on an efficient force field dedicated to the polyanions.

Mulliken charges of terminal oxygen atoms in hepta-anions do not vary from the gas phase to aqueous media, with a constant value of −0.81 for $[Mo_7O_{24}]^{6-}$ and −0.86 for $[W_7O_{24}]^{6-}$.[7] Significant changes are observed for pseudoterminal, two- and three-coordinate oxygens, with an increase in the negative charge. Schemes (a) and (b) in Figure 3 represent the Coulomb potential plotted on an isodensity molecular surface (0.001 e^- $bohr^{-3}$) for both gas-phase and aqueous environments. The potential is consistent with the variation of the Mulliken charges. Indeed, the solvent enhances the nucleophily of these three types of oxygen atoms, and the Coulomb potential in the vicinity of terminal oxygens is almost unchanged by the inclusion of water.

Alongside the interaction with solvent, these hepta-anions interact with their counterions. Out of computation necessity, vibrational calculations, detailed below, were performed by considering only one isolated aminopyridinium cation. As shown in Figure 3 (scheme e), however, the crystal structure of $(C_5H_7N_2)_6(Mo_7O_{24})\cdot 3H_2O$ obtained by X-ray diffraction[24] shows that at least four aminopyridinium cations and two water molecules interact with the heptamolybdate anion. Three types of hydrogen bonds can be isolated in this arrangement, N−H···O (2.71−3.20 Å), $N-H\cdots O_w$ (2.70−3.18 Å), and $O_w-H_w\cdots O$ (2.72−2.93 Å).[31] The oxygen atoms of the polyanion which are involved in the interactions with aminopyridinium are mostly the two-coordinate atoms O_1, O_3, and O_4. The terminal oxygen atoms interact predominately with water molecules. Four-coordinate oxygens like O_6 do not increase their Mulliken charges in aqueous media, but because of the proximity of the two-coordinate atoms, a nucleophilic nest appears close to them, as can be seen in Figure 3, scheme c, with the (−0.760 e^- $bohr^{-1}$) isopotential surface. Nevertheless, these atoms do not appear to interact with counterions or water molecules due to the steric hindrance of the cluster, which outweighs any favorable electrostatic effects created by the solvent. The two-coordinate atoms and the terminal oxygen atoms, which are also possible sites of interactions, as shown on the (−0.706 e^- $bohr^{-1}$) isopotential surface (Figure 3, scheme d), are more accessible and therefore interact preferentially with water molecules and aminopyridinium cations, resulting in the crystal structure shown in Figure 3, scheme e.

To summarize, it seems that the discrepancy found for some W−O bonds is not a consequence of any calculation artifact but is purely linked to the solvent effect, with a slight sensitivity to the theoretical model for W_2-O_2 bond. The role of the pseudoterminal atoms such as O_2 and the reason why $M-O_{pt}$ bonds are more sensitive to the solvent, especially for heptatungstate, are still unclear. A parallel with previous studies on octamolybdate isomers[3,32] may be illuminating. In these compounds, pseudo-four-coordinate atoms stand in for pseudoterminal oxygens. When interactions with the environment and counterions are considered, these atoms are four-coordinated, but when isolated, they tend toward three-coordinate. In heptapolyanions, the influence of the solvent leads to the pseudoterminal oxygen atoms becoming more strongly bonded to the metal atoms and hence becoming more genuinely bridging atoms.

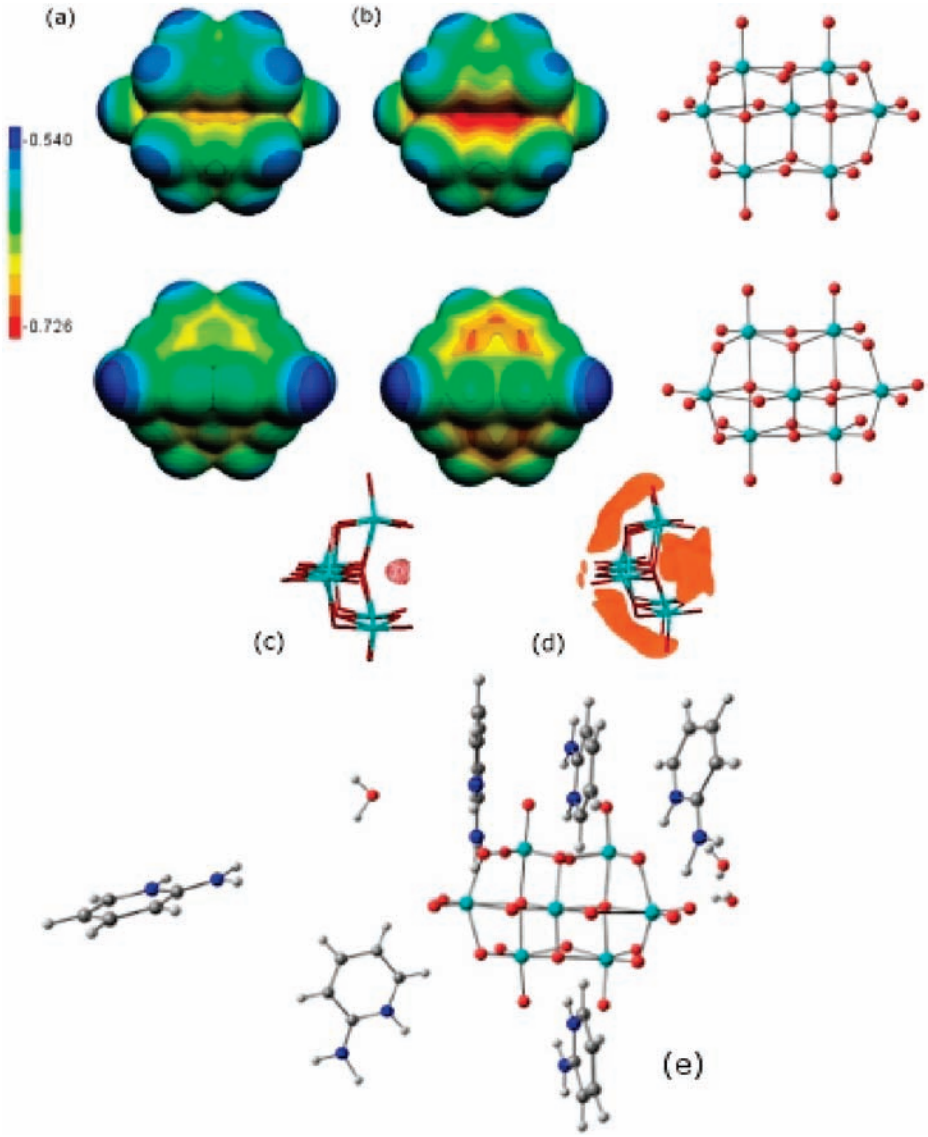

Figure 3. Isodensity molecular surface (0.001 e^- $bohr^{-3}$) colored in accordance to the Coulomb potential. Calculation of the potential in the gas phase (column a) and in water (column b) with two different views. Isopotential surfaces are also represented: −0.760 e^- $bohr^{-1}$ (c) and −0.706 e^- $bohr^{-1}$ (d). Also represented in (e) is $(C_5H_7N_2)_6(Mo_7O_{24})\cdot 3H_2O$, adapted from the crystal structure obtained by Román et al.[24]

Vibrational Spectrum of the $[Mo_7O_{24}]^{6-}$ Anion. ***General Remarks.*** Containing 31 atoms, this polyanion has 87 normal modes, which, for the C_{2v} symmetry, span the irreducible representations in eq 1, where Raman (R) and infrared (IR) activities are shown in parentheses.

$$\Gamma_{vib} = 26A_1(R, IR) + 18A_2(R) + 20B_1(R, IR) + 23B_2(R, IR) \quad (1)$$

The main calculated IR frequencies are listed in Table 3, where experimental frequencies proposed by Román et al.[24] and Isaac et al.[33] are also included. Computational results are compared to these two experiments using the root-mean-square (rms) error. The lowest rms is for the gas-phase calculations, with respect to Isaac's experiments; therefore, for the sake of clarity, only frequencies obtained in this environment are included in Table 3 (see the Supporting Information for the full list of calculated frequencies). The rms values are in the same range as those values obtained in a previous study on the $[Mo_6O_{19}]^{2-}$ anion,[7] though the assignment of the experimental $[Mo_7O_{24}]^{6-}$ vibrational frequencies is more complicated due to the lower symmetry allowing more modes to be infrared- and Raman-active. It is also interesting to note that for simple systems, ADF software gives, with the same level of theory, calculated IR frequencies around 4% lower than experimental results,[34] a difference which is very similar to the one obtained for the two anions.

Comparing the scalar with the spin−orbit ZORA approaches to assess the impact of these relativistic effects on vibrational frequencies leads to essentially identical frequencies. Independent of the level of theory, the only differences that appear in the calculated frequencies are more linked to the selected process for the differentiation of the first derivatives of the energy, that is, a numerical versus an analytical calculation. Even in that case, the largest difference, found in the spectrum for $[W_7O_{24}]^{6-}$ at around 200 cm^{-1} (ν_{39}), is only 6 cm^{-1}, which is small compared to the width of the bands in the experimental spectra.

The C_{2v} symmetry of $[Mo_7O_{24}]^{6-}$ leads to all 87 vibrations being potentially Raman-active. For the assignment, experimental data are taken from Aveston and co-workers and Griffith and co-workers, who performed Raman spectroscopy on a

TABLE 3: Calculated Spin−Orbit ZORA and Experimental IR Vibrational Frequencies (in cm^{-1}) for $[Mo_7O_{24}]^{6-}$ in the Gas Phase[a]

mode		calculated	observed		assignment
		gas phase	from ref 24	from ref 33	
A_1	ν_1	899 (160)	945		$\nu_s(Mo(O_t)_2)$; $\nu_s(Mo-O_{pt})$*
B_2	ν_{65}	884 (273)	935	930	$\nu_{as}(Mo(O_t)_2)$; $\nu_{as}(Mo-O_{pt})$*
B_1	ν_{45}	877 (162)			$\nu_{as}(Mo(O_t)_2)$
A_1	ν_2	871 (440)	915	920	$\nu_s(Mo-O_{pt},Mo-O_t)$
B_1	ν_{46}	853 (893)	890	895	$\nu_{as}(Mo-O_{2c},Mo-O_{3c},Mo-O_t)$
B_2	ν_{68}	832 (833)	875	880	$\nu_{as}(Mo-O_{pt},Mo-O_t)$
A_1	ν_5	816 (285)	860	865	$\nu_s(Mo-O_{pt},Mo-O_{3c},Mo-O_t)$; $\nu_s(Mo-O_{4c})$*
B_2	ν_{69}	804 (380)	845	835	$\nu_{as}(Mo-O_{pt},Mo-O_{3c},Mo-O_t)$; $\nu_{as}(Mo-O_{2c})$*
A_1	ν_6	715 (319)	685	760[b]	$\nu_s(Mo-O_{2c},Mo-O_{3c})$; $\nu_s(Mo-O_{4c})$
B_1	ν_{47}	686 (1084)	670	640[c]	$\nu_{as}(Mo-O_{2c},Mo-O_{4c})$; $\nu_{as}(Mo-O_{3c})$
B_2	ν_{71}	655 (1244)	650	600[c]	$\nu_{as}(Mo-O_{pt},Mo-O_{2c},Mo-O_{4c})$; $\nu_{as}(Mo-O_{3c})$*
B_1	ν_{49}	602 (91)	640[d], 635[d]		$\nu_{as}(Mo-O_{3c},Mo-O_{4c})$; $\delta_{as}(Mo-O_{2c})$
A_1	ν_8	556 (62)	560[d]	550[b]	$\delta_s(Mo-O_{2c},Mo-O_{3c},Mo-O_{4c})$
B_2	ν_{72}	528 (95)		515[b]	$\delta_{as}(Mo-O_{2c},Mo-O_{4c},Mo-O_t)$
A_1	ν_{10}	461 (48)	470		$\delta_s(Mo-O_{2c},Mo-O_{3c},Mo-O_{4c})$
B_1	ν_{51}	449 (80)	395	410[1]	$\delta_{as}(Mo-O_{2c},Mo-O_{4c},Mo-O_t)$
B_2	ν_{73}	434 (73)	360		$\delta_{as}(Mo-O_{pt},Mo-O_{3c},Mo-O_{4c})$
B_2	ν_{74}	399 (120)	325		$\delta_{as}(Mo-O_{2c},Mo-O_{3c},Mo-O_{4c},Mo-O_t)$
B_2	ν_{77}	332 (186)	295		$\delta_{as}(Mo-O_{2c},Mo-O_{3c},Mo-O_{4c})$
B_2	ν_{79}	246 (58)	265		contribution of all atoms

[a] The calculated IR intensities are also given in parentheses (in km mol^{-1}). An asterisk indicates a small contribution. [b] Assigned in reference 33 to MoO_6. [c] Assigned in reference 33 to pyridine. [d] Assigned in reference 24 to the breathing mode of the anion.

TABLE 4: Calculated Spin−Orbit ZORA and Experimental Raman Frequencies (in cm^{-1}) for $[Mo_7O_{24}]^{6-}$ in the Gas Phase[a]

mode		calculated	observed		assignment
		gas phase	from ref 35	from ref 38	
A_1	ν_1	899[b] (199)	934	938	$\nu_s(Mo(O_t)_2)$; $\nu_s(Mo-O_{pt})$*
B_2	ν_{65}	884[b] (65)	908	911	$\nu_{as}(Mo(O_t)_2)$; $\nu_{as}(Mo-O_{pt})$*
B_1	ν_{45}	877[b] (20)	890	893	$\nu_{as}(Mo(O_t)_2)$
A_1	ν_2	871[b] (28)			$\nu_s(Mo-O_{pt},Mo-O_t)$
B_2	ν_{66}	865 (30)	880		$\nu_{as}(Mo-O_{pt},Mo-O_t)$
A_1	ν_3	862 (66)			$\nu_s(Mo-O_{pt},Mo-O_t)$
B_2	ν_{67}	852 (49)	860	863	$\nu_{as}(Mo-O_{2c},Mo-O_t)$
A_1	ν_4	849 (92)			$\nu_s(Mo-O_{pt},Mo-O_t)$; $\nu_s(Mo-O_{2c})$*
A_2	ν_{28}	832 (4)	840	833	$\nu_s(Mo-O_{2c},Mo-O_t)$; $\nu_s(Mo-O_{4c})$*
B_2	ν_{68}	832[b] (46)			$\nu_{as}(Mo-O_{pt},Mo-O_t)$
A_1	ν_5	816[b] (19)			$\nu_s(Mo-O_{pt},Mo-O_t)$; $\nu_s(Mo-O_{3c},Mo-O_{4c})$*
A_2	ν_{29}	729 (4)			$\nu_s(Mo-O_{2c},Mo-O_{4c})$; $\nu_s(Mo-O_{3c})$*
A_1	ν_6	715[b] (6)			$\nu_s(Mo-O_{2c},Mo-O_{3c})$; $\nu_s(Mo-O_{4c})$*
B_1	ν_{48}	628 (7)	630	633	$\delta_{as}(Mo-O_{2c},Mo-O_{3c})$; $\nu_{as}(Mo-O_{4c})$
A_1	ν_9	519 (4)	550	543	$\delta_s(Mo-O_{2c},Mo-O_{3c},Mo-O_{4c})$
A_1	ν_{11}	415 (9)	450		$\delta_s(Mo-O_{pt},Mo-O_{3c},Mo-O_{4c})$
B_2	ν_{74}	399[b] (8)	415	375	$\delta_{as}(Mo-O_{2c},Mo-O_{3c},Mo-O_{4c})$
B_1	ν_{53}	353 (5)	363	363	$\delta_{as}(Mo-O_{2c},Mo-O_{3c},Mo-O_t)$
A_1	ν_{14}	347 (6)			$\delta_s(Mo-O_{pt},Mo-O_{2c},Mo-O_t)$
A_2	ν_{34}	333 (8)	340		$\delta_s(Mo-O_{pt},Mo-O_{3c},Mo-O_t)$
A_1	ν_{15}	312 (7)			
A_1	ν_{17}	268 (11)	308	308	
A_1	ν_{18}	235 (13)	245		
A_1	ν_{19}	207 (13)	220	223	
A_2	ν_{38}	203 (5)			
A_1	ν_{20}	197 (7)			
A_2	ν_{39}	192 (6)			
B_1	ν_{59}	190 (8)			
A_1	ν_{23}	112 (4)	115		

[a] The calculated Raman intensities are also given in parentheses (in $Å^4$ amu^{-1}). An asterisk indicates a small contribution. [b] Coincident with IR bands.

$(NH_6)_4Mo_7O_{24}\cdot 4H_2O$ and on a $(NH_4)_4Mo_7O_{24}\cdot 4H_2O$ crystal, respectively.[35,36]

Tables 3 and 4 include an approximate description of IR and Raman modes in terms of the stretching (ν) and bending (δ) of the bonds.

Analysis of the IR and Raman Spectral Traces. The IR and Raman spectral traces of the $[Mo_7O_{24}]^{6-}$ anion between 0 and 1100 cm^{-1} are shown in Figures 4 and 5, respectively. The calculated Raman spectral trace represents the sum of the anion and the aminopyridinium cation spectra; the experimental spectrum has been redrawn from that reported by Isaac et al.[33] For the assignment, they are conveniently divided into four blocks based on the different types of vibrations. These blocks are represented by dashed lines on the spectral traces. As shown

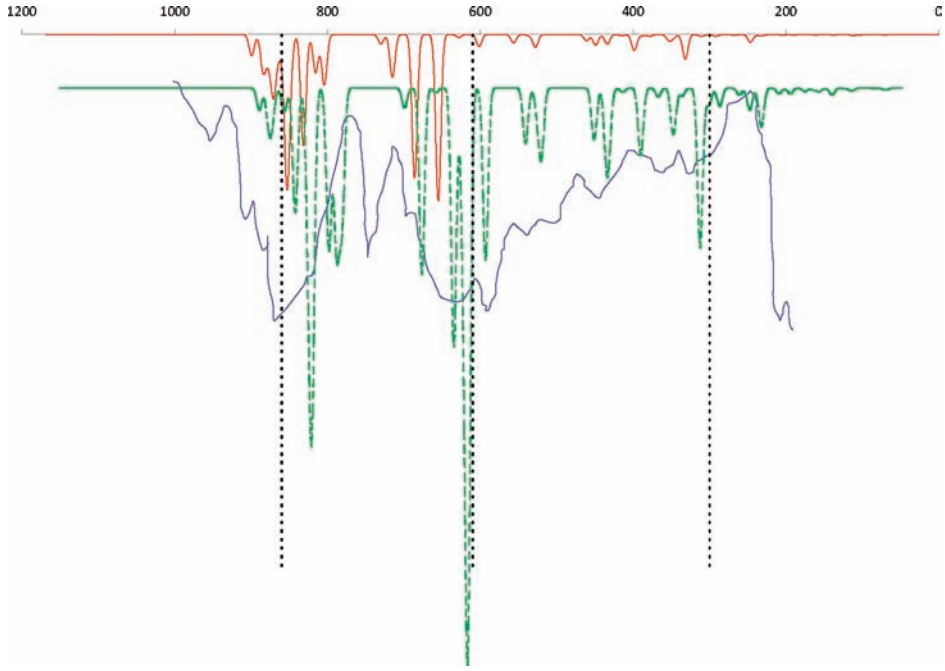

Figure 4. IR spectra for $[Mo_7O_{24}]^{6-}$. Calculated spectral traces in the gas phase (—) and in water (- - -). The experimental[33] and water spectral traces are shifted with respect to the *y* axis. Frequencies are given in cm^{-1}. The four blocks of frequencies are separated by dashed lines.

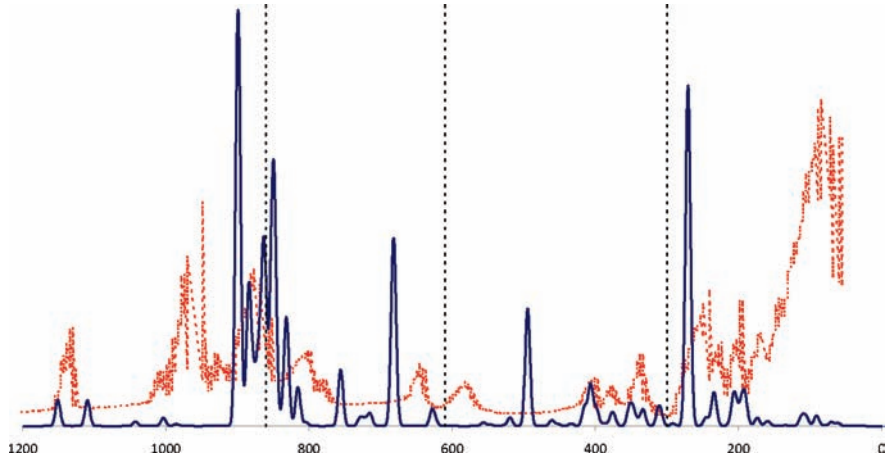

Figure 5. Raman spectra for $[Mo_7O_{24}]^{6-}$ and $(C_5H_7N_2)_6Mo_7O_{24}\cdot 3H_2O$. Calculated spectral trace in the gas phase (—) and the experimental spectrum (- - -) redrawn from Isaac and co-workers.[33] Frequencies are given in cm^{-1}. The four blocks of frequencies are separated by dashed lines.

in Figure 5, for Raman frequencies above 1000 cm^{-1}, the main contribution comes from the aminopyridinium cation, with peaks calculated at 1151, 1043, and 986 cm^{-1}. The first two bands are assigned by Isaac and co-workers to the bending of pyridine ring hydrogen atoms. The last peak obtained experimentally in this region, at around 990 cm^{-1}, is due to "breathing" of the pyridine ring.

The first IR block encompasses the high frequencies (>870 cm^{-1}). Four peaks at 899, 884, 877, and 871 cm^{-1} can be assigned to A_1 (ν_1), B_2 (ν_{65}), B_1 (ν_{45}), and A_1 (ν_2) modes, respectively. They involve symmetric (A_1) and asymmetric (B_2) stretching of metal−terminal oxygen bonds. Stretching motions involving the pseudoterminal atoms also contribute to these vibrational modes, contrary to the assignment by Lyhamn, who suggested that the stretching motions of the terminal oxygen atoms do not mix with other vibrational modes.[37] For $[Mo_6O_{19}]^{2-}$, theses modes vibrate at higher frequencies,[7] which is consistent with the smaller charge of the anion.[38]

Experimentally, bands are also observed in this region of the IR spectrum (Figure 4). Isaac et al. found only two peaks at 930 and 920 cm^{-1}, and these can be assigned to B_2 (ν_{65}) and A_1 (ν_2) modes. Román and co-workers, who did not provide a spectral trace, observed three peaks at higher frequencies. Lyhamn, who measured IR and Raman spectra on a $Na_6Mo_7O_{24}\cdot 14H_2O$ single crystal, detected two bands at 952 and 939 cm^{-1} [37] in this region, whereas Griffith et al. reported only one weak band at 917 cm^{-1}. The first Raman block, with four intense bands, matches exactly the IR spectra and can be readily assigned to stretching of $M-O_t$ bonds with a small contribution from pseudoterminal oxygen atoms. Aveston and Griffith's results are very similar, with frequencies higher than the calculated one.

IR absorptions between 804 and 853 cm^{-1} are due to stretches of Mo_2O_2 and Mo_3O_3 units, $Mo-O_{2c}$, $Mo-O_{3c}$, and $Mo-O_t$ bonds (B_1 (ν_{46}) asymmetric mode) and $Mo-O_{pt}$ and $Mo-O_t$ (B_2 (ν_{68})). For modes A_1 (ν_5) and B_2 (ν_{69}), there is a contribution from $Mo-O_{3c}$ bonds. For Román et al., this range has the same amplitude but higher frequencies ([845;890] cm^{-1}). Isaac et al. reported four peaks in this block, at 895, 880, 865, and 835 cm^{-1}. They noted a peak at 760 cm^{-1}, which they assigned to

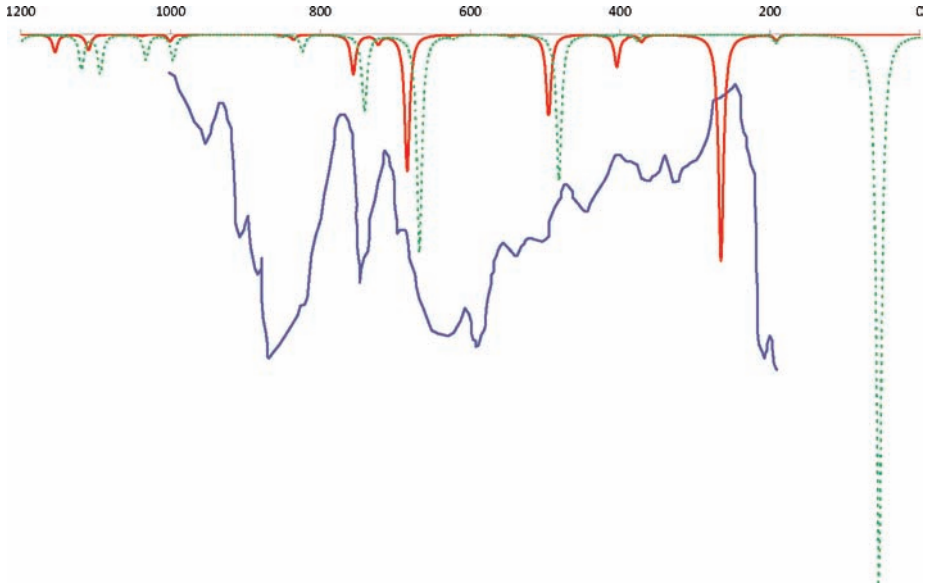

Figure 6. Comparison of the calculated IR spectrum for the aminopyridinium ion in the gas phase (—) and in water (- - -) with $(C_5H_7N_2)_6Mo_7O_{24}\cdot 3H_2O$ (shifted —) redrawn from ref 33. Frequencies are given in cm^{-1}.

an asymmetric stretching mode of MoO_6 octahedra. This band could match the calculated frequency at 715 cm^{-1} due to the symmetric stretching mode A_1 (ν_6) or the asymmetric stretching modes B_2 at 804 cm^{-1}. However, the spectral trace of the aminopyridinium ion, shown in Figure 6, has a peak at exactly 760 cm^{-1}. Therefore, the experimental band seems more likely to be due to the cation $[C_5H_7N_2]^+$ than the polyanion.

In the second Raman block, all of the calculated peaks between 715 and 865 cm^{-1} are included, and some peaks which are very close in frequency contribute to the same band. Aveston and co-workers reported three bands, at 880, 860, and 840 cm^{-1}, which correspond to the band on the experimental spectral trace (Figure 4) at approximately 850 cm^{-1}. Griffith et al. had only two peaks at 863 and 833 cm^{-1}. The experimental assignment for $[Mo_7O_{24}]^{6-}$ is made difficult by a peak due to the aminopyridinium cation at 855 cm^{-1}, which occurs nearly at the same Raman frequency as the B_2 (ν_{67}) asymmetric mode.

The next two strong IR bands calculated at 686 and 655 cm^{-1} match well the two peaks found by Román et al. at 670 and 650 cm^{-1}. Isaac et al. also reported two "very strong bands" in this region, at 640 and 600 cm^{-1}. They assigned them to the in-plane ring deformation of the aminopyridinium cation. It is clear in Figure 6 that there are no peaks around these frequencies due to the cation. One peak appears at 680 cm^{-1}, but it matches better the peak reported at 705 cm^{-1} and assigned to C−H out-of-plane deformation of the cation, in accordance with the work reported here.

The third block begins with the B_1 (ν_{49}) mode at 602 cm^{-1} for the IR spectrum and the B_1 (ν_{48}) mode at 628 cm^{-1} for the Raman spectrum. For these two modes, stretching and bending both contribute to the vibrational modes. The Raman spectrum of the cation exhibits two peaks in this block. The first one at 626 cm^{-1} was identified by Isaac et al. at around 625 cm^{-1}. One calculated band due to the B_1 $[Mo_7O_{24}]^{6-}$ (ν_{61}) mode appears at a similar frequency of 628 cm^{-1}. A second Raman peak due to the cation at 546 cm^{-1} is very close to the band assigned to the anion by Aveston et al. at 550 cm^{-1} and that at 543 cm^{-1} by Griffith et al. Román and co-workers noted two IR peaks at 640 and 635 cm^{-1} and assigned them to the breathing modes of the polyanion. However, they do not match well with any calculated peaks. At 627 cm^{-1}, a small IR peak appears for the aminopyridinium cation in water, and this could give rise to one of the experimentally observed bands, although Román reported that the bands are strong. At this point, their assignment cannot readily be explained using the separate cation−anion model used here.

At 556 cm^{-1}, the theoretical IR spectrum exhibits a medium band due to the symmetric bending A_1 (ν_8) mode involving $Mo-O_{2c}$, $Mo-O_{3c}$, and $Mo-O_{4c}$ bonds. This assignment corresponds with that of Isaac and co-workers at 550 cm^{-1}. They also assigned the observed band at 515 cm^{-1} to a symmetric bending mode. It could match the B_2 (ν_{72}) mode calculated at 528 cm^{-1}. However, the aminopyridinium spectrum indicates that the peak at 515 cm^{-1} is actually due to the cation, corresponding to the peak calculated at 496 cm^{-1}. The same arguments could be made with the peak at 410 cm^{-1}, assigned by Isaac and co-workers to an asymmetric bending mode. It could match the peak observed by Román et al. at 395 cm^{-1} and calculated at 449 cm^{-1}. Again, the contribution of the aminopyridinium cation in that range of frequencies makes the assignment more complicated because another of its bands appears at 406 cm^{-1}. The band observed at 410 cm^{-1} is probably due to $[C_5H_7N_2]^+$ and not to the heptamolybdate anion as suggested by Isaac et al. In the third block, only one Raman peak coincides with an IR band at 399 cm^{-1} and is assigned to a bending asymmetric B_2 (ν_{74}) mode. The aminopyridinium Raman spectral trace shows a very weak peak at 388 cm^{-1} which matches the band assigned to the cation by Isaac et al. at around 375 cm^{-1}.

For frequencies with $\nu < 300$ cm^{-1}, more Raman spectral data than IR modes have been reported. They are mostly due to symmetric motions and, according to Isaac and co-workers, arise from translations and rotations of MoO_6 groups. They involve movements of all of the atoms. Thus, assignments to individual functional groups become less clear.

Influence of the Solvent on the IR and Raman Spectra. Figure 4 shows the spectral trace of $[Mo_7O_{24}]^{6-}$ obtained with the inclusion of solvent in the computational modeling. Calculations were performed on the COSMO-optimized geometry of the anion. The rms over the whole range of meaningful frequencies [0;1100] cm^{-1} is higher than that when solvent is not included. This is especially noticeable when the data of

TABLE 5: Characteristic Group Frequencies (in cm^{-1}) for Type-I and Type-II POMs Based on Experimental Results

		α- and β-$[XMo_{12}O_{40}]^{z-}$		$[Mo_6O_{19}]^{2-}$		$[XMo_6O_{24}]^{z-}$		$[Mo_7O_{24}]^{6-}$
ν(X–O)	IR	940–1060			R	680–685		
	IR	800–960			IR	540–635		
ν(Mo–O_t)	R	960–999	R	980–999	R	900–960	R	890–940
	IR	920–980	IR	957–970	IR	900–960	IR	915–945
	R	920–980	R	951–968				
ν(Mo–O_{pt})							R	830–880
							IR	600–900
ν(Mo–O_{2cI}–Mo)	R	600–630			R	690–720	R	830–880
	IR	700–810	IR	796–810	IR	690–720	IR	600–900
ν(Mo–O_{2cII}–Mo)	IR	770–900						
ν(Mo–O_a)	R	245–247	R	278–290				

Román are used. Solvent leads to a shift of the spectral trace toward lower frequencies and an increase in the calculated IR intensity, especially for the strongest bands ν_{47} and ν_{71}. These results confirm the observations made for $[TeMo_6O_{24}]^{8-}$ and $[IMo_6O_{24}]^{5-}$ anions.[10] In the previous study, an analysis of the bond order revealed a decrease in the covalent character of metal−oxygen bonds upon solvation. Associated with an increase in the bond dipole moment, this explained these two effects of solvation. As shown in Figure 6, solvation also leads to the aminopyridinium IR spectrum being shifted toward lower frequencies with a very large shift of the low-energy peak from 265 cm^{-1} in the gas phase to 55 cm^{-1} in an aqueous environment.

The calculated frequencies of the bending modes in the gas phase were higher than Román's results, giving a rms value of 51 cm^{-1}. The shift of these frequencies in water is such that the rms decreases to 40 cm^{-1}. Finally, it may be noted that contrary to $[Mo_6O_{19}]^{2-}$, inclusion of the solvent does not increase the vibrational frequencies due to stretching of Mo−O_t bonds.[10]

Vibrational Sspectrum of the $[W_7O_{24}]^{6-}$ Anion. The calculated IR and Raman spectral traces of the $[W_7O_{24}]^{6-}$ anion are represented in Figure 9 (Supporting Information). Frequencies obtained in the gas phase and with solvent were determined using the same level of theory as for $[Mo_7O_{24}]^{6-}$. C_{2v} symmetry was confirmed by the structural analysis and lack of imaginary frequencies. A similar spectrum to the heptamolybdate anion's is expected, but as pointed out by Thouvenot et al., the molybdate framework has a reduced rigidity compared to that of tungsten.[39] Hence, force constants associated with metal−oxygen bonds are expected to be higher, leading to a shift toward higher vibrational frequencies. This shift is confirmed on the spectral trace, with a first band at 928 cm^{-1}, for the symmetric stretching mode A_1 (ν_1), assigned to stretching of W−O_t bonds. A peak was observed by Himeno et al. at 944 cm^{-1} and could match this first calculated band. A band which occurs at 912 cm^{-1} contributes to the band at 915 cm^{-1}. It is assigned to the asymmetric stretching mode B_2 (ν_{65}).

The four blocks assigned for the $[Mo_7O_{24}]^{6-}$ anion are also identifiable on the spectral trace of heptatungstate based on the nature of the vibrations. The few experimental data available do not allow a thorough comparison with experiment. Although some calculated Raman frequencies match the bands reported by Himeno et al., the influence of the acetonitrile used as the solvent and the counterion induces a shift which makes the assignment uncertain. However, the analysis of $[Mo_7O_{24}]^{6-}$ vibrational modes suggests the assignments reported in the Supporting Information. The main IR bands obtained in the gas phase are summarized and compared to the experimental values reported by Himeno and co-workers.[40] The spectrum of these workers was recorded for a $Cs_6W_7O_{24}\cdot 5H_2O$ solution, and only a few bands were reported in the range of [400;1300] cm^{-1}.

Conclusion

The structures of $[Mo_7O_{24}]^{6-}$ and $[W_7O_{24}]^{6-}$ isopolyanions have been refined, achieving a better computational−experimental agreement than that achieved previously. This improvement is made possible by the combined use of a new geometry optimization algorithm available in ADF2008 and an improvement in the level of theory based on DFT. It has been shown that, even for heptatungstate, spin−orbit coupling has little effect on the calculated structural and vibrational properties compared to a scalar treatment. This conclusion suggests that an efficient computational strategy for closed-shell polyanions can safely neglect spin−orbit effects.

Moreover, the need for incorporation of environmental effects using solvent models has been confirmed when ($q/m \geq 0.8$), especially for structural studies. Nevertheless, as Bagno and co-workers underlined, "the influence of the solvent cannot be overemphasized".[26] Indeed, even though metal−terminal oxygen bond lengths are improved slightly, some tungsten−oxygen bonds which involve pseudoterminal oxygen atoms are found to be very sensitive to the interactions with the solvent and can shorten considerably in water. This result may have important consequences for other polyanions containing pseudoterminal atoms and weakly bonded oxygens but also for other systems with long weak bonds.

The vibrational study of $[Mo_7O_{24}]^{6-}$ and $[W_7O_{24}]^{6-}$ confirms the sensitivity of the vibrational trace to the solvent. The observed shifts toward lower frequencies for the polyanions are in accord with previous work. For isolated polyoxoanions, the pseudoterminal oxygens contribute to M−O_t vibrations between 890 and 940 cm^{-1}, and their main IR and Raman modes appear between 600 and 880 cm^{-1}. Table 5 summarizes the characteristic group frequencies for type-I and type-II polyoxometalates, including those with pseudoterminal atoms. Results obtained for the heptamolybdate are compiled with previous vibrational frequencies found for α- and β-$[XMo_{12}O_{40}]^{z-}$, $[Mo_6O_{19}]^{2-}$, and $[XMo_6O_{24}]^{z-}$.[10]

The spectra obtained for the isolated anions are in good agreement with previous experimental studies, especially because experiments are often performed on the solid state. Moreover, large organic counterions are often used experimentally to stabilize polyoxometalate phases; therefore, to model better the crystal environment, assignment of vibrational frequencies of polyanions must include the counterion. The contribution of the aminopyridinium ion led to ambiguity in the experimental assignments, many of which have been resolved by combining calculations of the polyanion and counterion. However, the interaction between the cation and anion no doubt further complicates the spectra, and although computationally demanding, a complete assignment will require both ions and their interactions.

Evaluation of the binding energies between the cation and the anion could provide information that would fully characterize the types of interactions that occur between the polyanions and their counterions but also with their environment such as water molecules. It could also clarify the influence of the pseudoterminal oxygens regarding the reactivity of hepta-anions.

Acknowledgment. The authors thank the Australian Research Council for financial support.

Supporting Information Available: Additional results. This material is available free of charge via the Internet at http://pubs.acs.org.

References and Notes

(1) Pope, M. *Heteropoly and Isopoly Oxometalates*; Springer: Heidelberg, Germany, 1983.
(2) Pope, M.; Müller, A. *Angew. Chem., Int. Ed. Engl.* **1991**, *30*, 34.
(3) Bridgeman, A.; Cavigliasso, G. *Inorg. Chem.* **2002**, *41*, 3500.
(4) Tytko, K. H.; Mehmke, J.; Fischer, S. *Bonding and Charge Distribution in Isopolyoxometalate Ions and Relevant Oxides A Bond Valence Approach*; Springer: Berlin, Heidelberg, Germany, 1999; Vol. 93.
(5) Bridgeman, A.; Cavigliasso, G. *J. Chem. Soc., Dalton Trans.* **2002**, 2244.
(6) Bridgeman, A.; Cavigliasso, G. *Inorg. Chem.* **2002**, *41*, 1761.
(7) Bridgeman, A.; Cavigliasso, G. *Chem. Phys.* **2002**, *279*, 143.
(8) Bridgeman, A. *Chem. Phys.* **2003**, *287*, 55.
(9) Bridgeman, A. *Chem.—Eur. J.* **2004**, *10*, 2935.
(10) Bridgeman, A. *Chem.—Eur. J.* **2006**, *12*, 2094.
(11) Vosko, S.; Wilk, L.; Nusair, M. *Can. J. Phys.* **1980**, *58*, 1200.
(12) Becke, A. D. *Phys. Rev. A* **1988**, *38*, 3098.
(13) Perdew, J. P. *Phys. Rev. B* **1986**, *33*, 8822.
(14) *ADF2008.01*; SCM, Theoretical Chemistry, Vrije Universiteit: Amsterdam, The Netherlands, 2008.
(15) te Velde, G.; Bickelhaupt, F.; van Gisbergen, S.; Fonseca Guerra, C.; Baerends, E.; Snijders, J.; Ziegler, T. *J. Comput. Chem.* **2001**, *22*, 931.
(16) Fonseca Guerra, C.; Snijders, J.; te Velde, G.; Baerends, E. *Theor. Chem. Acc.* **1998**, *99*, 391.
(17) Swart, M.; Bickelhaupt, F. *Int. J. Quantum Chem.* **2006**, *106*, 2536.
(18) van Lenthe, E.; Baerends, E.; Snijders, J. *J. Chem. Phys.* **1993**, *99*, 4597.
(19) van Lenthe, E.; Baerends, E.; Snijders, J. *J. Chem. Phys.* **1994**, *101*, 9783.
(20) van Lenthe, E.; Ehlers, A.; Baerends, E. *J. Chem. Phys.* **1999**, *110*, 8943.
(21) Klamt, A.; Schüürmann, G. *J. Chem. Soc.: Perkin Trans.* **1993**, *2*, 799.
(22) Pye, C.; Ziegler, T. *Theor. Chem. Acc.* **1999**, *101*, 396.
(23) Ikenoue, S.; Mikuriya, M.; Miyauchi, O.; Nukada, R.; Yagasaki, A. *Bull. Chem. Soc. Jpn.* **1994**, *67*, 2590.
(24) Román, P.; Gutiérrez-Zorrilla, J. M.; Martínez-Ripoll, M.; García-Zorilla, S. *Transition Met. Chem.* **1986**, *11*, 143.
(25) López, X.; Fernández, J.; Romo, S.; Paul, J. F.; Kazansky, L.; Poblet, J. M. *J. Comput. Chem.* **2004**, *25*, 1542.
(26) Bagno, A.; Bonchio, M.; Autschbach, J. *Chem.—Eur. J.* **2006**, *12*, 8460.
(27) Fernández, J. A.; López, X.; Poblet, J. M. *J. Mol. Catal. A: Chem.* **2007**, *262*, 236.
(28) López, X.; Nieto-Draghi, C.; Bo, C.; Bonet Avalos, J.; Poblet, J. M. *J. Phys. Chem. A* **2005**, *109*, 1216.
(29) Berendsen, H. J. C.; Grigera, J. R.; Straasma, T. P. *J. Phys. Chem.* **1987**, *91*, 6269.
(30) Jaramillo, P.; Pérez, P.; Fuentealba, P.; Canuto, S.; Coutinho, K. *J. Phys. Chem. B* **2009**, *113*, 4314.
(31) Román, P.; Gutiérrez-Zorrilla, J. M.; Luque, A.; Martínez-Ripoll, M. *J. Crystallogr. Spectrosc. Res.* **1988**, *18*, 117.
(32) Bridgeman, A. *J. Phys. Chem. A* **2002**, *106*, 12151.
(33) Isaac, M.; Pradip, T.; Nayar, V. *J. Solid State Chem.* **1994**, *112*, 132.
(34) Fan, L.; Ziegler, T. *J. Chem. Phys.* **1992**, *96*, 9005.
(35) Aveston, J.; Anacker, E.; Johnson, J. *Inorg. Chem.* **1964**, *3*, 735.
(36) Griffith, W.; Lesniak, P. *J. Chem. Soc. A* **1969**, 1066.
(37) Lyhamn, L. *Acta Chem. Scand. A* **1982**, *36*, 595.
(38) Hardcastle, F.; Wachs, I. *J. Raman Spectrosc.* **1990**, *21*, 683.
(39) Thouvenot, R.; Fournier, M.; Franck, R.; Rocchiccioli-Deltcheff, C. *Inorg. Chem.* **1984**, *23*, 598.
(40) Himeno, S.; Yoshihara, M.; Maekawa, M. *Inorg. Chim. Acta* **2000**, *298*, 165.

JP9063438